Robust Model Predictive Control With Simplified Repetitive Control for Electrical Machine Drives

Ying Liu, Shanmei Cheng, Bowen Ning, and Yesong Li

***Abstract*—Conventional model predictive control (MPC) for electrical drives relies on the accuracy of system model, thus, its performance will deteriorate due to disturbances such as parameter mismatch and current distortion. To improve the robustness of MPC, a compensated scheme with simplified repetitive control (SRC) is proposed in this paper. Since the prediction of MPC is corrected with the assistance of compensation, a much more reasonable output is provided to promote system performance. An open-loop structure of repetitive control (RC) with two resonant units is applied for the proposed SRC to guarantee stability and maintain high accuracy for tracking disturbances, and moreover, SRC responds fast and just needs half of the data memory used by an ideal RC. Additionally, an output filter is designed to correct the quantizing error of frequency, thus, the frequency adaption is enhanced. To validate the feasibility and the effectiveness of the proposed method, a compensated MPC for permanent-magnet synchronous machine drive system is utilized. Both simulation and experiment results prove significant performance enhancement of the SRC-based robust MPC, and compared with the conventional MPC, it provides nearly 30% reduction of total harmonic distortion (THD) in stator phase current.**

***Index Terms*—Disturbances suppress, electrical machine, model predictive control (MPC), repetitive control (RC).**

I. Introduction

MODEL predictive control (MPC) has been extensively investigated in fast dynamic control systems [1]–[3]. MPC applied to the drive system for electrical machines, such as the permanent-magnet synchronous machine (PMSM), will maintain fast response in the transient state and reduced current and torque ripple in the steady-state. Some modulated MPC strategies have been proposed to promote the system performance [4], [5]. In which, the space vector modulation (SVM) is used to synthesize the voltage vector and to obtain fixed switching frequency. Theoretically, MPC outperforms many other high efficient strategies, e.g., field-oriented control and direct torque

Manuscript received April 12, 2018; revised June 6, 2018; accepted July 16, 2018. Date of publication July 19, 2018; date of current version March 29, 2019. Recommended for publication by Associate Editor J. Rodriguez. *(Corresponding author: Shanmei Cheng.)*

Y. Liu, S. Cheng, and Y. Li are with the Key Laboratory of Image Processing and Intelligent Control, School of Automation, Huazhong University of Science and Technology, Wuhan 430074, China (e-mail:

integral (PI) controller is applied to RC to promote system stability and robustness against parameter variations [18]–[21]. Since a weighting factor is added to RC, the strength of a resonant unit in suppressing disturbances will be deteriorated. A modified RC using one-sixth of fundamental period as delay time is proposed in [18] for three-phase grid-connected inverters. A plug-in type is applied in this scheme, and the RC is combined with a PI regulator to reinforce the system performance and provide high amplitude gain for the fundamental component. This method can achieve fast responses and perfect harmonic suppression performance. However, it is just effective for the $(6n \pm 1)$th harmonics but has no effects on other harmonics.

The ideal RC can be decomposed as an integrator and infinite orders of resonant units operating in parallel. To guarantee system stability, the gain of the integrator must be limited when the input contains dc components. Since the integrator and the resonant unit share the same gain, which are coupled with each other, the strength in tracking harmonics will be significantly deteriorated when a small gain is configured for RC. To overcome this drawback, a simplified RC (SRC) with an open-loop structure is proposed in this paper. For the new method, the transfer function between the output of the controller and disturbances does not contain an integrator block but consists of a series of resonant units. Thus, a large amplitude gain for tracking harmonic components is maintained because the dc drifts and harmonics can be removed separately with the proposed method.

For the control of electrical machines, the fundamental frequency changes during operation. Besides, a fractional value of quantized frequency is rounded to the nearest integer because RC cannot exactly track noninteger frequency. To improve the tracking performance of time-varying periodic references, several frequency adaptive RC (ARC) methods [23]–[26] are put forward. An improved ARC with frequency adaption is proposed in [23], where a new fractional-order RC (FORC) with a high-order finite impulse response filter is applied to approximate the fractional delay. Besides, more FORC schemes are investigated in [27]–[29]. Although the ARC methods can minimize periodic disturbances, an accurate frictional model in FORC seems too complicated to be applied for the MPC-based drive system. Thus, a more efficient scheme is applied in this paper to promote the tracking performance of time-varying and noninteger frequency.

Since the disturbances in the MPC-based electrical drive system are repetitive for every fundamental cycle, an SRC based on an open-loop RC structure and combined with feed-forward compensation scheme is proposed in this paper to improve the robustness of MPC against disturbances. The new proposed SRC method provides fast response, enhanced stability, and promoted tracking ability. This paper is organized as follows. Section II introduces the MPC-based PMSM drive system, and the effects of disturbances on MPC are theoretically analyzed. Section III presents the proposed SRC with an open-loop structure, and moreover, the quantizing error of frequency is corrected with an output filter. Detailed simulation and experiment results are presented in Sections IV and V, respectively. Conclusions are presented in Section VI.

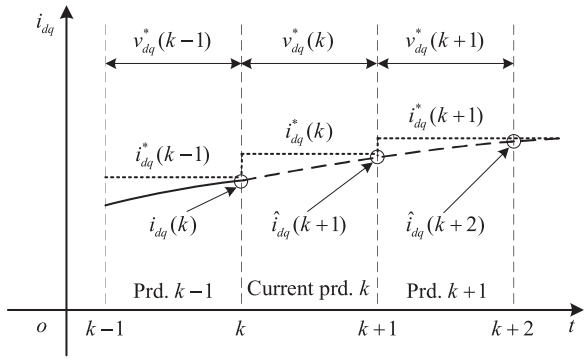

Fig. 1. Control sequence of the MPC method.

II. MPC FOR PMSM DRIVE SYSTEM

A. PMSM Model for MPC System

The PMSM is widely researched because of its advantages such as high efficiency, high-power density, high-power factor, low temperature rise, and good dynamic performance [6], [7], [9]. In this paper, the surface-mounted PMSM is utilized for the implementation and verification of the proposed method. The current function of the PMSM is described [6], [7] as follows:

$$\dot{i}_{dq}(t) = L_s^{-1}[v_{dq}(t) - R_s i_{dq}(t) - j\omega_e \varphi_{dq}(t)] \tag{1}$$

where $v_{dq} = v_d + jv_q$ and $i_{dq} = i_d + ji_q$ represent the stator voltage vector and the current vector in synchronous rotating coordinate *dq*; symbol *j* represents the imaginary part of a complex variable. R_s and L_s are stator resistance and inductance of the electrical machine, respectively; ω_e is an equivalent electrical angular frequency in stator reference frame, and $\varphi_{dq} = \varphi_d + j\varphi_q$ is the stator flux vector as shown in the following equation:

$$\varphi_{dq}(t) = L_s i_{dq}(t) + \phi_m \tag{2}$$

where ϕ_m is the amplitude of magnet flux.

When the sampling time T_s is small enough, changes in speed and position are neglected, and the rotor speed keeps constant in few periods. A discrete current prediction is acquired in (3) with the assistance of first-order Taylor series expansion

$$\hat{i}_{dq}(k+1) = i_{dq}(k) + L_s^{-1} T_s[v_{dq}(k) - R_s i_{dq}(k) - j\omega_e \varphi_{dq}(k)] \tag{3}$$

where $\hat{i}_{dq}(k+1)$ is the predictive current vector at the beginning of next period $k+1$, and $\varphi_{dq}(k)$ is calculated through (2) with the measured current $i_{dq}(k)$. Since there is one-step delay for PWM updating, a two-step prediction of MPC is performed to compensate this delay. The control sequence of the MPC method is presented in Fig. 1, in which, the dead-beat method is applied and it forces the prediction $\hat{i}_{dq}$ approaching to the reference i^*_{dq} at the end of period $k+1$, as $\hat{i}_{dq}(k+2) = i^*_{dq}(k+1)$. Based on the following equation, the predictive current $\hat{i}_{dq}(k+2)$ at

the end of next period $k+1$ can be calculated as

$$\hat{i}_{dq}(k+2) = \hat{i}_{dq}(k+1) + L_s^{-1}T_s\Big[v_{dq}^*(k+1) - R_s\hat{i}_{dq}(k+1) - j\omega_e\hat{\varphi}_{dq}(k+1)\Big] \quad (4)$$

where $\hat{\varphi}_{dq}(k+1)$ is the estimated flux calculated with the predicted current $\hat{i}_{dq}(k+1)$as $\hat{\varphi}_{dq}(k+1) = L_s\hat{i}_{dq}(k+1) + \phi_m$. The reference voltage $v_{dq}^*(k+1)$ as shown in the following equation can be acquired by solving (4), and then an SVM is utilized to produce the required switch states. It is clear that the voltage target is calculated in current period *k* and will be applied during the coming period, thus, the one-step delay is compensated

$$v_{dq}^*(k+1) = R_s\hat{i}_{dq}(k+1) + L_sT_s^{-1}\Big[i_{dq}^*(k+1) - \hat{i}_{dq}(k+1)\Big] + j\omega_e\hat{\varphi}_{dq}(k+1). \quad (5)$$

The reference current is usually assumed to be constant in few steps, as $i_{dq}^*(k+1) = i_{dq}^*(k)$ for convenience. However, the performance of electrical drives will be improved by simply taking the trend of reference into consideration. An estimation method with specified damping coefficient k_i is applied to obtain the reference in the next period as

$$i_{dq}^*(k+1) - i_{dq}^*(k) = k_i\left[i_{dq}^*(k) - i_{dq}^*(k-1)\right]. \quad (6)$$

The reference current can be derived in the following equation. The estimate reference will be convergent when the constraint $0 < k_i < 1$ for damping coefficient fulfills. The original assumption $i_{dq}^*(k+1) = i_{dq}^*(k)$ will also hold in the steady-state because the references in last two periods are the same

$$i_{dq}^*(k+1) = (1+k_i)i_{dq}^*(k) - k_ii_{dq}^*(k-1). \quad (7)$$

B. Disturbances in MPC

MPC strategy can provide high-performance control for the PMSM drive system with the assistance of accurate system model. However, the exits of disturbance will significantly deteriorate the system performance. The effects on MPC for certain major disturbances including the parameter mismatch, current distortion, and deadtime effects are analyzed as follows.

1) Mismatch of Machine Parameter: Parameters of PMSM such as stator resistance R_s, stator inductance L_s, and amplitude of magnet flux ϕ_m will mismatch with their theoretical values during operation due to the changes of temperature and magnate saturation. As a consequence, disturbances will be introduced to the predictive current when the parameters mismatch. The predictive current $\hat{i}_{dq}(k+1)$ varies with time when the mentioned parameters change, and the relationship can be described as

$$\frac{d}{dt}\hat{i}_{dq}(k+1) = \left(\frac{\partial}{\partial R_s}\frac{dR_s}{dt} + \frac{\partial}{\partial L_s}\frac{dL_s}{dt} + \frac{\partial}{\partial \phi_m}\frac{d\phi_m}{dt}\right)\cdot\hat{i}_{dq}(k+1). \quad (8)$$

The disturbance Δi_{dq} is defined as $\Delta i_{dq} = \hat{i}'_{dq} - \hat{i}_{dq}$, where $\hat{i}'_{dq}$ stands for the predictive current with mismatched parameters $R'_s = R_s + \Delta R_s$, $L'_s = L_s + \Delta L_s$, and $\phi'_m = \phi_m + \Delta\phi_m$, and ΔR_s, ΔL_s, and $\Delta\phi_m$ represent the cumulative increment of stator resistance, stator inductance, and amplitude of magnet flux, respectively. Instituting (3) into (8), and the disturbance Δi_{dq} can be acquired as follows:

$$\begin{aligned}\Delta i_{dq}(k+1) &= \int d\hat{i}_{dq}(k+1)/dt \\ &= L_s^{-1}T_s[-\Delta R_s i_{dq}(k) - j\omega_e\Delta L_s i_{dq}(k) \\ &\quad - j\omega_e\Delta\phi_m] - \Delta L_s L_s^{-1}[\hat{i}_{dq}(k+1) - i_{dq}(k)].\end{aligned} \quad (9)$$

Errors between the predictive and measured currents and also between the reference and real current will be introduced, and as a consequence, the final voltage vector cannot be precisely predicted by MPC.

2) Current Distortion: Current drifts are unavoidable for measured stator current due to the offset in analog detecting circuits, and besides, mismatches will be introduced to the amplitude of current because of the inaccuracy of resistance, load effects, and noises in the detecting circuits. Moreover, current distortion occurs during the transient state such as speed step and load torque step conditions. The measured stator currents with dc drifts and amplitude mismatches can be described as follows:

$$\begin{cases} i_a = I\sin\omega_e t \\ i_b = I\sin(\omega_e t - 2\pi/3) \\ i_c = I\sin(\omega_e t + 2\pi/3) \end{cases}, \quad \begin{cases} i'_a = (1+k_a)i_a + \Delta I_a \\ i'_b = (1+k_b)i_b + \Delta I_b \\ i'_c = (1+k_c)i_c + \Delta I_c \end{cases} \quad (10)$$

where i_a, i_b, and i_c represent the theoretical stator currents with amplitude *I* and angular frequency ω_e, while i'_a, i'_b, and i'_c are measured values coupled with dc drifts ΔI_{abc} and amplitude mismatches $k_{abc}I$. The coordinate transform $\mathbf{T_{3s/2r}}$ as shown in (11) is used to turn these currents to synchronous rotating coordinate, thus $i_{dq} = \mathbf{T_{3s/2r}}\cdot i_{abc}$. The current disturbances in *dq*-axes are described in (12), where A_n and δ_n are the amplitude and phase of the *n*th ($n = 0, 1, 2$) order harmonics

$$\mathbf{T_{3s/2r}} = \frac{2}{3}\begin{bmatrix} \sin\omega_e t & \sin\left(\omega_e t - \frac{2}{3}\pi\right) & \sin\left(\omega_e t + \frac{2}{3}\pi\right) \\ -\cos\omega_e t & -\cos\left(\omega_e t - \frac{2}{3}\pi\right) & -\cos\left(\omega_e t + \frac{2}{3}\pi\right) \end{bmatrix} \quad (11)$$

$$\begin{aligned}\Delta i_{dq}(t) &= \mathbf{T_{3s/3r}}\cdot(i'_{abc} - i_{abc}) \\ &= A_0 + A_1\sin(\omega_e t + \delta_1) + A_2\sin(2\omega_e t + \delta_2).\end{aligned} \quad (12)$$

The order of frequency spectrum will be shifted by left and by right for one unit after the harmonic transforming from stationary coordinate to synchronous rotating coordinate. Thus, when distortion exists in the detected current, the disturbances Δi_{dq} in MPC are presented dc offset and current ripple including the fundamental component and the second-order harmonic associated with frequency ω_e.

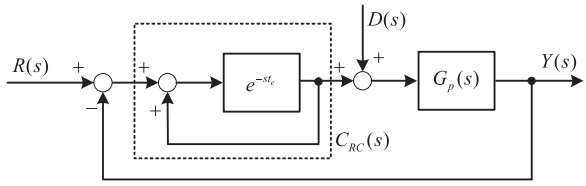

Fig. 2. General closed-loop control system based on RC.

3) Deadtime Effects: Deadtime is necessary in power electronic devices used by PMSM drives and it will produce series of harmonics. Even though these deadtime-induced harmonics are quite small, the predictive error will be amplified when the predicting step increases and their effects on control system cannot be neglected to obtain high-performance control. As researched in [13] and [18], the deadtime contributes to $(6n \pm 1)$th harmonics in stationary coordinate. The detailed distribution of harmonic in both stationary and synchronous rotating coordinate is presented as follows:

$$\begin{cases} \Delta i_{abc}(t) = (h_5 + h_7) + (h_{11} + h_{13}) + (h_{17} + h_{19}) + \cdots \\ \Delta i_{dq}(t) = (h_4 + h_6 + h_8) + (h_{10} + h_{12} + h_{14}) \\ \qquad\qquad +(h_{16} + h_{18} + h_{20}) + \cdots \\ h_n(t) = A_n \sin(n\omega_e t + \delta_n). \end{cases} \tag{13}$$

In summary, the predictive and measured currents contain large amounts of disturbances under conditions such as parameter mismatch, current distortion, and deadtime effects. The form of disturbances Δi_{dq} in MPC as shown in the following equation is presented as dc offset and series of harmonics associated with the electrical rotating frequency ω_e:

$$\Delta i_{dq}(t) = A_0 + \sum_n A_n \sin(n\omega_e t + \delta_n). \tag{14}$$

III. Proposed SRC With MPC

The predictive current will mismatch with the real current due to the existence of disturbances, as a consequence, large distortion and excitation will be introduced to both of the output current and electromagnetic torque. This is not permitted in the control of high-performance electrical drives, thus, an efficient controller is necessary to improve the performance of the MPC-based drive system. The RC controller is widely utilized dealing with periodic signals, since the disturbances present as series of harmonics and repeat for every fundamental cycle, a compensated MPC with SRC is proposed in this paper to suppress these disturbances.

A. Conventional RC

A general closed-loop control system based on the ideal RC controller is presented in Fig. 2, where *R*(*s*), *Y*(*s*), and *D*(*s*) are the input reference, output, and disturbance, respectively; G_p(s) stands for the control plant, and $C_{\mathrm{RC}}(s)$ is an ideal RC controller.

The internal model theory declares that the tracking error will asymptotically converge to zero for any input *R*(*s*) and disturbance *D*(*s*) under the circumstance that the controller contains all unstable poles of both *R*(*s*) and *D*(*s*). The unstable components in input and disturbance are equivalently transformed to *D*(*s*) for convenience. According to the analysis in Section II-B, the disturbance *D*(*s*) consists of dc drifts and series of harmonics associated with frequencies ω_e, as

$$D(s) = L[\Delta i_{dq}(t)] = s^{-1}A_0 + \sum_n A_n \omega_e \Big/ \left[s^2 + (n\omega_e)^2\right]. \tag{15}$$

Based on the internal model theory, the ideal RC controller $C_{\mathrm{RC}}(s)$ as shown in the following equation is used to suppress these harmonics:

$$\begin{aligned} C_{\mathrm{RC}}(s) &= \exp(-2\pi s/\omega_e)/\left[1 - \exp(-2\pi s/\omega_e)\right] \\ &= -0.5 + t_e^{-1}s^{-1} + 2t_e^{-1}\sum_{n=1}^{\infty} s \Big/ \left[s^2 + (n\omega_e)^2\right] \end{aligned} \tag{16}$$

where $t_e = 2\pi/\omega_e$ is the fundamental period, and the time-delay module $\exp(-2\pi s/\omega_e)$ or $\exp(-st_e)$ is the so-called internal model. The ideal RC consists of three parts operating in parallel, i.e., a proportional block with negative coefficient, an integrator, and the infinite numbers of resonant units with frequencies $n\omega_e$. The negative proportional block may affect the stability of the control system while the pure integrator and resonant units will produce poor stability during applications. Besides, the ideal RC delays about one fundamental period that it provides slow response speed. Thus, a modified RC as shown in the following equation is commonly adopted in applications to promote the stability and dynamical performance [18]–[21]

$$\begin{aligned} C'_{\mathrm{RC}}(s) &= 1 + k_r C_{\mathrm{RC}}(s) \\ &= (1 - 0.5k_r) + k_r t_e^{-1}s^{-1} \\ &\quad + 2k_r t_e^{-1}\sum_{n=1}^{\infty} s \Big/ \left[s^2 + (n\omega_e)^2\right] \end{aligned} \tag{17}$$

where $0 < k_r < 2$ is the weighting factor evaluated with a positive constant.

However, the performance of RC will be deteriorated when dc components exist because the strength of the integrator unit on dc drifts is the same or comparable as that of the resonant unit on harmonics at the resonant frequency ω_e as shown in the following equation:

$$\lim_{s\to j0^+} k_r t_e^{-1}s^{-1} \Big/ \lim_{s\to j\omega_e^+} \left[2k_r t_e^{-1} s/(s^2 + \omega_e^2)\right] = 1.0. \tag{18}$$

To guarantee the stability of the RC-based system, the gain $k_r t_e^{-1}$ of integrator must be limited when the dc drifts exist in disturbance, thus, the tracking ability of the resonant unit is significantly suppressed simultaneously. Under this circumstance, the advantages of RC in eliminating harmonics will be sacrificed.

B. Proposed SRC

An SRC is proposed in this paper, where an open-loop RC structure with the internal model $\exp(-st_e)$ is applied to

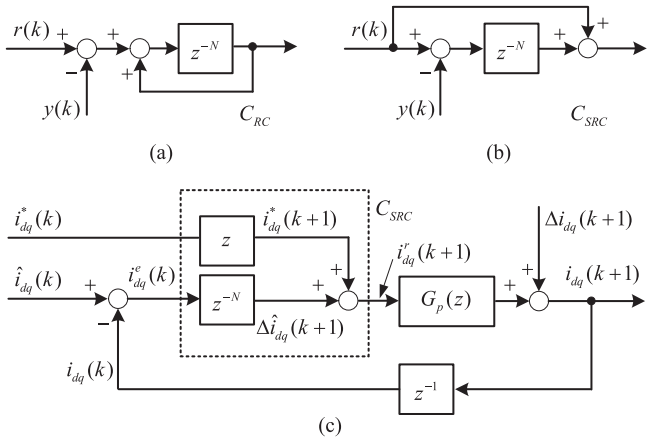

Fig. 3. Signal flowcharts of the RC, proposed SRC, and SRC-based MPC system. (a) Ideal RC. (b) Proposed SRC. (c) SRC-based MPC system.

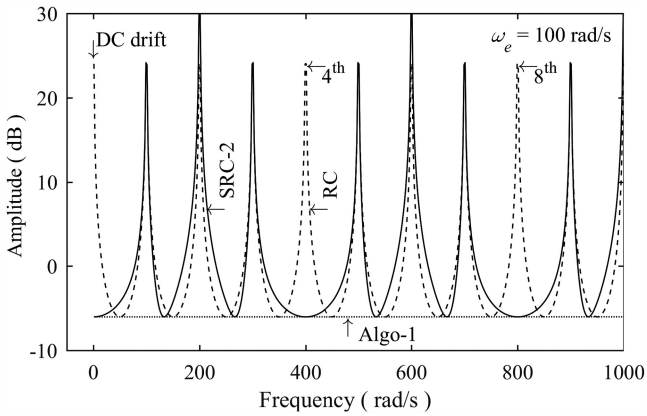

Fig. 4. Frequency responses of the conventional RC, Algo-1, and proposed SRC-2.

suppress the disturbances. Signal flowcharts of the ideal RC [see Fig. 3(a)], proposed SRC [see Fig. 3(b)], and SRC-based MPC control system [see Fig. 3(c)] are presented in Fig. 3. Where $N = t_e/T_s$ is the quantity of fundamental period, i^e_{dq} is the predictive error between the predictive current $\hat{i}_{dq}$ and measured current i_{dq}, i^r_{dq} is the current command after compensating. A continuous SVM is applied to the control system, and the deadtime effects and other disturbance are transformed to the disturbance Δi_{dq}, thus, the PMSM model can be simplified as $G_p(z) = 1$. The new proposed SRC method as shown in Fig. 3(a) is different from the conventional RC controller [see Fig. 3(b)] which constructs a closed-loop structure with a feedback path, whereas the new method produces an open-loop structure with feed-forward compensation. Since the dead-beat strategy as shown in Fig. 1 is applied to the system, the predictive and reference current will intersect at the end of each period as $i^*_{dq}(k) = \hat{i}_{dq}(k)$. The predictive error is send to SRC and the output compensation $\Delta\hat{i}_{dq}$ is added to the reference in the implemented SRC and MPC-based drive system. Compared with the conventional RC, the new proposed SRC avoids the negative impacts mentioned in Section III-A and it provides an enhanced ability in eliminating harmonics.

The principle of the proposed SRC-based MPC system can be expressed as

$$\begin{cases} \Delta\hat{i}_{dq}(k+1) = z^{-N}\left[\hat{i}_{dq}(k) - z^{-1}i_{dq}(k+1)\right] \\ i^r_{dq}(k+1) = i^*_{dq}(k+1) + \Delta\hat{i}_{dq}(k+1). \end{cases} \tag{19}$$

The dead-beat strategy ensures $i^*_{dq}(k+1) = \hat{i}_{dq}(k+1)$, instituting it into (19) and the transfer function between compensation $\Delta\hat{i}_{dq}$ and disturbance Δi_{dq} of the proposed SRC method can be derived as

$$Q(z) = \Delta\hat{i}_{dq}(k)/\Delta i_{dq}(k) = -z^{-N}/(1+z^{-N}). \tag{20}$$

The amplitude of $Q(z)$ is as follows:

$$\|Q(z)\| = 1/\sqrt{2[1+\cos(2\pi\omega/\omega_e)]}. \tag{21}$$

It clearly shows that SRC is a resonant unit with the resonant frequencies $(0.5+n)\omega_e$, ($n = 0, 1, 2, \ldots$). Defining a kth order resonant unit $P_k(z)$ as

$$P_k(z) = z^{-N/(2k)}/[1+z^{-N/(2k)}]. \tag{22}$$

Thus, the resonant frequencies of $P_k(z)$ are $(1+2n)k\omega_e$. The proposed SRC can be decoupled as a series of resonant units operating in parallel as shown in the following equation and it covers all orders of frequencies $k\omega_e$:

$$-Q(z) = P_1(z) + P_2(z) + P_4(z) + P_8(z) + \cdots. \tag{23}$$

The strength of harmonic decreases rapidly as the harmonic order increases, and the quantizing error will increase when the order of resonant unit $P_k(z)$ rises. Thus, a reduced order SRC controller C_{SRC-2} with the first- and the second-order resonant units is utilized as shown in (24) to simplify the system structure. The SRC-2 is only lacking of resonant frequencies $4k\omega_e$ compared with the complete controller as shown in (23); however, it significantly reduces the complication of the SRC-based control system

$$\begin{cases} -Q_{\mathrm{SRC}-2}(z) = P_1(z) + P_2(z) \\ C_{\mathrm{SRC}-2}(z) = z^{-N/2} + z^{-N/4}. \end{cases} \tag{24}$$

Besides, Siami *et al.* [11] proposed a compensation algorithm (Algo-1) as shown in the following equation to suppress disturbance:

$$\begin{cases} \Delta\hat{i}_{dq}(k+1) = k_f\left[\hat{i}_{dq}(k) - z^{-1}i_{dq}(k+1)\right] \\ i^r_{dq}(k+1) = i^*_{dq}(k+1) + \Delta\hat{i}_{dq}(k+1). \end{cases} \tag{25}$$

The predictive current error in the last period is used as compensation and k_f is the weighting factor of this compensation. It is evaluated with a positive constant less than unit to ensure stability. For the Algo-1 method, the transfer function between compensation and disturbance can be derived as

$$\begin{cases} -Q_{\mathrm{Algo}-1}(z) = -\Delta\hat{i}_{dq}(k)/\Delta i_{dq}(k) = k_f/(1+k_f) \\ C_{\mathrm{Algo}-1}(z) = k_f. \end{cases} \tag{26}$$

Frequency responses of the conventional RC, Algo-1, and the proposed SRC-2 method are presented in Fig. 4. The proposed SRC-2 method provides large amplitude gains and enhanced tracking abilities at the resonant frequencies, and the

dc drifts issue introduced by conventional RC as mentioned in Section III-A has been canceled because the resonant gain for dc component is intentionally removed in SRC-2. Besides, comparing Algo-1 with the proposed SRC-2 method, the former one will introduce tracking error in the steady-state, whereas SRC-2 can obtain much better tracking performance with the benefits of resonant unit. The SRC-2 and Algo-1 method are equivalent when dealing with the dc drifts and harmonics at $4k\omega_e$ because SRC-2 is lacking of resonant units at these frequencies.

C. Compensation of Quantizing Error

To promote the stability of the control system, the output filter of RC is usually evaluated with a constant value, a first-order low-pass filter, a high-order Butterworth low-pass filter, or probably a finite impulse filter [18]–[22]. Besides, since a digital processor is adopted to quantize the resonant frequency, quantizing error will be introduced when the fundamental period t_e cannot be completely divided by the sampling period T_s because the number of sampling point is limited to an integer. Thus, the phase error will be introduced due to the inaccuracy of quantizing for fundamental frequency. For these reasons, an output filter with phase compensation is designed to ensure stability and to correct the phase error for SRC. The *k*th order SRC unit $C_{\mathrm{SRC}}(k,\ z)$ and its phase are presented in the following equations, respectively:

$$C_{\mathrm{SRC}}(k,z) = z^{-N/(2k)} \tag{27}$$

$$\angle C_{\mathrm{SRC}}(k,j\omega) = -0.5k^{-1}\cdot\omega t_e \tag{28}$$

where *N* is the quantized integer of fundamental period t_{e}.

Assuming that $(2kN + D)T_s$ is the theoretical quantizing result of t_e with the sampling time T_s, where D is the fractional component. An integer *N* nearest to $t_e/(2kT_s)$ is selected to provide the least approximating error, thus, the actually implemented fundamental period is $2kNT_s$, and the residual part is limited to $-0.5 < D < 0.5$. The quantizing phase error can be derived as

$$\Delta\angle C_{\mathrm{SRC}}(k,j\omega) = -0.5Dk^{-1}\cdot\omega T_s. \tag{29}$$

To correct this quantizing error, a phase compensation block V_k is proposed in (30) and its phase is given in (31)

$$V_k(z) = (1-0.5Dk^{-1}) + 0.5Dk^{-1}z^{-1} \tag{30}$$

$$\begin{aligned}\angle V_k(j\omega) = &-a\tan\left\{0.5Dk^{-1}\sin(\omega T_s)/[1-0.5Dk^{-1}\right.\\ &\left.+0.5Dk^{-1}\cos(\omega T_s)]\right\}.\end{aligned} \tag{31}$$

Since the frequencies of lower harmonics are far less than the sampling frequency as $\omega T_s \ll 2\pi$, the phase of V_k can be simplified as

$$\angle V_k(j\omega) = -0.5Dk^{-1}\cdot\omega T_s. \tag{32}$$

It clearly shows that the phase error is corrected as $\angle V_k(j\omega) = \Delta\angle C_{\mathrm{SRC}}(k,j\omega)$. The implementation of V_k is presented in (33), and the proposed resonant unit $P_k(z)$ after compensating is shown in (34)

$$\begin{cases} V_k(z) = (1-0.5Dk^{-1}) + 0.5Dk^{-1}z^{-1} \\ N = \mathrm{round}\left[t_e/(2kT_s)\right] \\ D = t_e/T_s - 2kN \end{cases} \tag{33}$$

$$P_k(z) = z^{-N/(2k)}\cdot V_k(z)\Big/\Big[1+z^{-N/(2k)}\cdot V_k(z)\Big]. \tag{34}$$

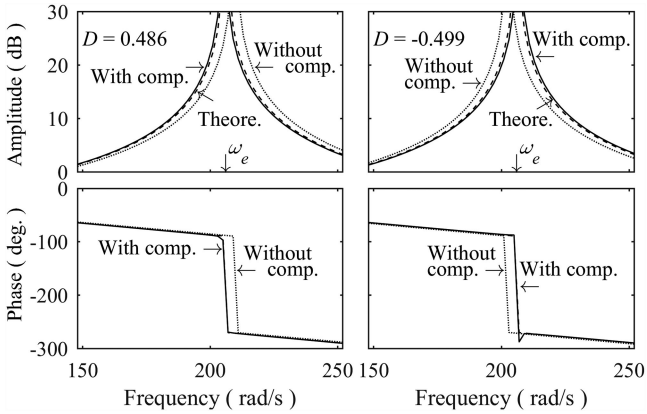

Fig. 5. Phase compensation for resonant unit $P_2(z)$.

The frequency response of $P_2(z)$ with corresponding phase compensations are presented in Fig. 5. The quantizing error of the fundamental frequency causes the implemented frequency departing from the theoretical one without compensation. For instance, the digital implementation of fundament period produces a quantizing error $D = 0.486$, as a result, the implemented resonant frequency shifts to the right side of the theoretical frequency before compensating. When the proposed compensation V_k is applied, the finally implemented frequency is almost the same as the theoretical value. The proposed phase compensation block succeeds to correct both positive and negative quantizing errors as Fig. 5 shows, thus, the tracking accuracy of the resonant frequency for the proposed SRC is promoted.

D. Implementation of SRC in MPC-Based PMSM Drives

Structures of the proposed compensated SRC-2 and the MPC-based PMSM drive system using this method are presented in Fig. 6. The open-loop SRC with two resonant units (SRC-2) and phase compensation are utilized as shown in the following equation and Fig. 6(a):

$$C_{\mathrm{SRC-2}}(z) = k_r\left[z^{-N/2}V_1(z) + z^{-N/4}V_2(z)\right] \tag{35}$$

where a positive constant coefficient k_r is provided to ensure system stability.

Compared with the conventional RC, the proposed SRC-2 contributes to a simplified structure and maintains much higher tracking accuracy for harmonics, and moreover, it provides faster response speed and just needs half of the memory occupied by the conventional RC. The proposed SRC-2 can be easily implemented in the MPC-based PMSM drive system as presented in Fig. 6(b), in which, an original current command i^*_{dq} is produced by a general PI speed regulator, and then the

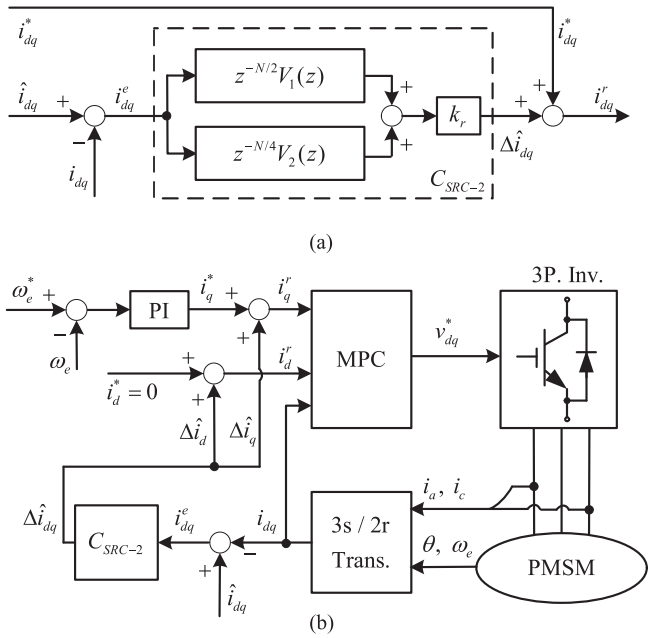

Fig. 6. Structures of the proposed SRC-2 and its implementation in MPC-based PMSM drives. (a) Proposed SRC-2 method. (b) MPC-based PMSM drives.

predictive current error is send to SRC-2 as input. The output compensation $\Delta\hat{i}_{dq}$ is added to the reference to generate the final current command i^r_{dq}. Based on this compensated current command, MPC controller generates the needed stator voltage v^*_{dq} to drive the PMSM machine. The predictive current is corrected that it helps MPC producing a much more reasonable output voltage, thus, the system's robustness against disturbance is significantly enhanced.

Considering the analysis in Section III-B [see (19)], the proposed SRC method for MPC-based PMSM drives can be described as

$$i^r_{dq}(k+1) = i^*_{dq}(k+1) + C_{\mathrm{SRC}-2}\left[\hat{i}_{dq}(k) - i_{dq}(k)\right]. \quad (36)$$

The PMSM model is simplified as $G_p(z) = 1$ and $i^r_{dq} = i_{dq}$ will hold, while the dead-beat strategy forces $i^*_{dq}(k+1) = \hat{i}_{dq}(k+1)$, thus, the predictive error i^e_{dq} of the proposed SRC-based control system can be derived as

$$i^e_{dq}(k+1) = \hat{i}_{dq}(k+1) - i_{dq}(k+1) = (-C_{\mathrm{SRC}-2})^{k+1} i^e_{dq}(0) \quad (37)$$

where $i^e_{dq}(0)$ is the initial value of predictive error. To guarantee the stability of the SRC and MPC-based PMSM drive system, the amplitude of C_{SRC-2} should be limited inside the unit circle. Taking (35) into consideration, the stable conditions can be acquired as

$$\|C_{\mathrm{SRC}-2}(z)\| < 1 \Rightarrow 0 < k_r < 0.5. \quad (38)$$

IV. Simulation Results

The MPC-based PMSM drive system is built to validate the proposed SRC method through simulation in MATLAB\Simulink. The system parameters are listed in Table I. To prove the efficiency of the proposed SRC method,

TABLE I
Parameters of the MPC-Based PMSM Drive System

Parameter	Symbol	Value
Pole Pairs	n_p	4
Stator Resistance	R_s	0.338 Ω
Stator Inductance	L_s	1.515 mH
Magnet Flux Amp.	Φ_m	0.0884 Wb
Nominal Speed	n_N	3000 rpm
Nominal Current	I_N	8.0 A
Load Current	I_L	6.3 A
DC Link Voltage	U_{dc}	150 V
Sampling Period	T_s	100 us
Deadtime	t_d	3 us
Gain of Algo-1	k_f	0.80
Gain of SRC-1	k'_r	0.80
Gain of SRC-2	k_r	0.40
Coefficient of Ref.	k_i	0.75

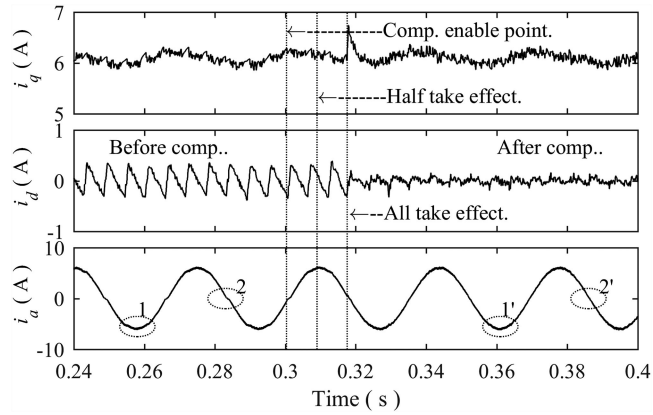

Fig. 7. Simulated stator currents before and after compensating using SRC-2 with injected current distortion ($n = 500$ r/min).

comparisons are conducted under the same circumstances for the four methods including the conventional MPC method (Conv.), the Algo-1 method as shown in (25), the proposed SRC-1 method with the first-order resonant unit as shown in the following equation, and the SRC-2 method with the first- and second-order resonant unit as shown in (35):

$$C_{\mathrm{SRC}-1}(z) = k'_r \cdot z^{-N/2} V_1(z). \quad (39)$$

To validate the effectiveness of the proposed SRC method with external disturbances, dc current drifts with 1.25% of the nominal current I_N are added to i_a, i_b, and i_c, and moreover, 15% amplitude distortion is injected into i_c as shown in the following equation. The detailed simulation results are presented as follows:

$$i'_a = i_a + 1.25\% \cdot I_N, \quad i'_b = i_b - 1.25\% \cdot I_N,$$
$$i'_c = 1.15 \cdot i_c + 1.25\% \cdot I_N. \quad (40)$$

The simulated stator currents of PMSM with injected current distortion before and after compensating using SRC-2 are presented in Fig. 7, in which, the compensation provided by SRC-2 is suddenly added at 0.3 s. Before compensating, currents in *dq*-axes are excited rapidly with harmonic frequencies ω_e due

TABLE II
SIMULATED CURRENT FREQUENCY SPECTRUMS (%) OF STATOR CURRENT WITH INJECTED CURRENT DISTORTION ($I_L = 4.0$ A, $N = 1500$ r/min)

Controller	DC	2nd	4th	5th	7th
Conv.	0.32	1.37	0.44	2.71	1.43
Algo-1	0.14	1.41	0.38	1.76	0.85
SRC-1	0.37	1.13	0.38	1.50	0.59
SRC-2	0.12	0.95	0.25	0.56	0.30
Controller	11th	13th	17th	19th	THD
Conv.	0.72	0.52	1.11	0.67	3.75
Algo-1	0.23	0.56	1.13	0.72	3.10
SRC-1	0.24	0.41	0.76	0.46	2.56
SRC-2	0.23	0.28	0.32	0.30	2.11

to the existences of disturbances, and the current is distorted at peaks and zeros as markers "1" and "2" indicate, respectively. However, the current ripple in i_d is significantly reduced after the compensation taking effects, and the current distortion is obviously promoted as markers "1'" and "2'" show. Most importantly, SRC-2 takes effects in a quarter of fundamental period after the compensation is enabled, and significantly changes are observed in half of fundamental period after compensating. Thus, SRC-2 responds faster than the ideal RC which delays for one fundamental period as theoretically analyzed.

The simulated harmonic spectrums of stator current with injected current distortion for the four methods are presented in Table II. The four systems operate at the same conditions with control frequency $f_s = 10$ kHz and speed command $n = 1500$ r/min, and the maximum considered harmonic frequency is 5.0 kHz. The Algo-1 method performs well in eliminating the fifth, seventh, and 11th harmonics which are mainly caused by the deadtime effects, but it cannot efficiently suppress the second, 13th, 17th, and 19th harmonics. Results show that both SRC-1 and SRC-2 method outperform Algo-1 method in eliminating harmonics. The fact that SRC-2 with two resonant units performs better than SRC-1 with one unit also indirectly proves the effectiveness of the proposed SRC method. Moreover, SRC-2 significantly suppresses all kinds of harmonics and obtains the least current total harmonic distortion (THD), for instance, it provides 43.7% reduction of THD compared with the conventional MPC.

Additionally, the THD of stator current for all-speed regions with injected current distortion is presented in Table III. It clearly shows that SRC-2 is effective in wide speed ranges and produces the least THD among the four methods. For lower speeds less than 150 r/min (10 Hz), the proposed SRC method is essentially the same as the Algo-1 method because of the limitation of predefined memory size $N = 1000$ (10 kHz/10 Hz). The effective speed range in low-speed region can be easily extended by increasing the memory size but may probably lead to increased costs.

Besides, the effectiveness of the proposed SRC method is separately verified through simulation with mismatched

TABLE III
SIMULATED THD (%) OF STATOR CURRENT FOR ALL-SPEED REGIONS WITH INJECTED CURRENT DISTORTION ($I_L = 6.3$ A)

Controller	300 rpm	500 rpm	800 rpm	1200 rpm	1500 rpm
Conv.	5.56	5.28	4.72	4.10	4.06
Algo-1	3.57	3.50	3.43	3.62	3.45
SRC-1	3.34	3.43	3.30	3.03	2.85
SRC-2	2.36	2.44	2.51	2.23	2.35

parameters, which include the stator resistance R_s, stator inductance L_s, and magnet flux ϕ_m as shown in (41). The simulated stator currents of PMSM with these mismatches are presented in Fig. 8. The compensation provided by SRC-2 is suddenly added to system at 0.3 s, and for all the three cases, the current ripple and distortion introduced by parameter mismatches are significantly reduced after the compensation taking effects. Simulation results prove that the proposed SRC-2 method can efficiently promote the parameter robustness of the MPC-based PMSM drive system

$$\begin{cases} \text{case 1: } R'_s = 4.0R_s \\ \text{case 2: } L'_s = 0.85L_s \\ \text{case 3: } \phi'_m = 0.85\phi_m . \end{cases} \tag{41}$$

V. EXPERIMENTAL RESULTS

A digital signal processer (DSP) named TMS320F28335 is used as the core of MPC-based PMSM drive system to implement the proposed SRC method. The detailed setup of experimental platform is presented in Fig. 9, in which, two PMSMs are driven by independent electrical drives operating in opposite directions, and they are coaxially connected and fixed by a coupler to emulate the load condition. System parameters of experiment are the same with that of simulation as shown in Table I. To validate the effectiveness of the proposed SRC method, PMSM drive systems with three methods including the conventional MPC method (Conv.), the Algo-1 method as shown in (25), and the proposed SRC-2 method are compared under the same conditions. The variables are sampled and stored into a specified memory with a sampling frequency 10 kHz which is the same as the control frequency. Thus, the information for every control step is completely recorded during operation, and then all stored signals are read out and drawn aligned with time sequence.

To validate the ability of proposed SRC in suppressing current disturbances, external current distortion as shown in (40) is injected for experiment. The PMSM starts from standstill and enters the steady-state with speed command $n = 1500$ r/min and load current 6.3 A, and then, the reference speed suddenly jumps from 1500 to 500 r/min at 2.0 s. The speed and current in dq-axes during starting up and braking are presented in Fig. 10. All methods operate properly with external disturbance and during speed up and down processes. Moreover, SRC-2 responds faster than other two methods as shown in Fig. 10(a) during starting up, for instance, to reach the reference speed, SRC-2

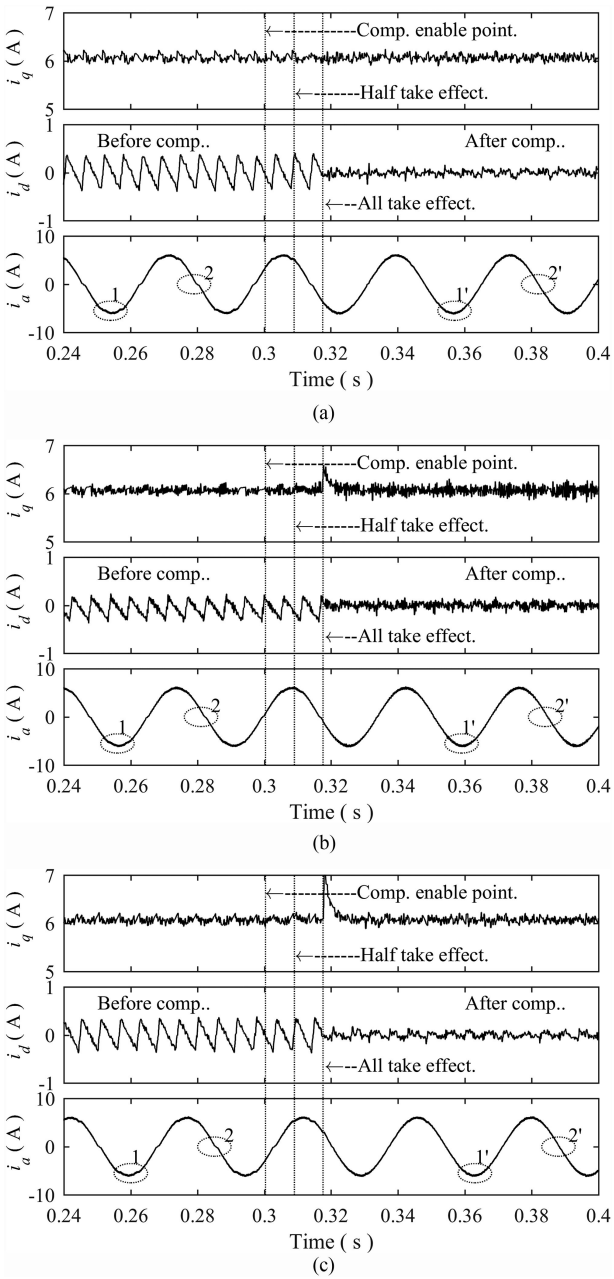

Fig. 8. Simulated stator current before and after compensating using SRC-2 with parameter mismatch (n = 500 r/min). (a) Case 1: 4.0 R_s. (b) Case 2: 0.85 L_s. (c) Case 3: 0.85 Φ_m.

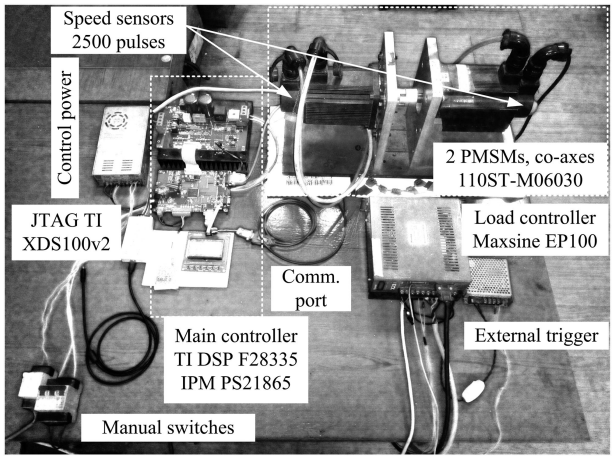

Fig. 9. Experiment platform of the MPC-based PMSM drive system with the proposed SRC method.

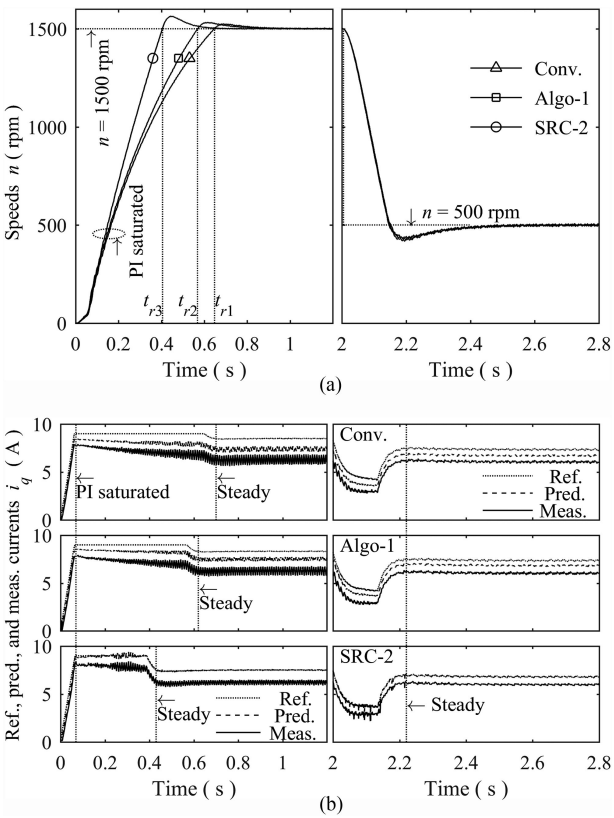

Fig. 10. Experimental speed and stator current during starting up and braking with injected current distortion. (a) Rotor speed. (b) Stator current i_q in q-axis.

uses time $t_{\mathrm{r}3} = 0.38$ s which is nearly 60% of time $t_{r1} = 0.66$ s used by the conventional MPC. When the PMSM starts from standstill, the output of a PI controller, namely, the current reference is increasing with time as Fig. 10(b) shows. The controllers enter saturated state and their references keep constant (9.0 A) as specified by the limitation of PI. Errors between the references and actual currents are observed due to the existence of disturbances. SRC-2 produces the least tracking error compared with Algo-1 and the conventional MPC. Most importantly, the current reference of SRC-2 converges to the predictive current when the compensation is enabled as theoretically analyzed in Section III-B.

The experimental stator currents and corresponding frequency spectrums for the three MPCs with injected current distortion are presented in Fig. 11. The detailed frequency spectrums of stator current for the three MPCs are presented in Table IV. The PMSMs are operating with speed command $n =$ 1500 r/min and load current 6.3 A. Comparative results illustrate that SRC-2 produces the least current ripple and tracking error in both d- and q-axis among the three methods. The reference current of SRC-2 strictly follows the predictive current, and a much more accurate current command is produced after

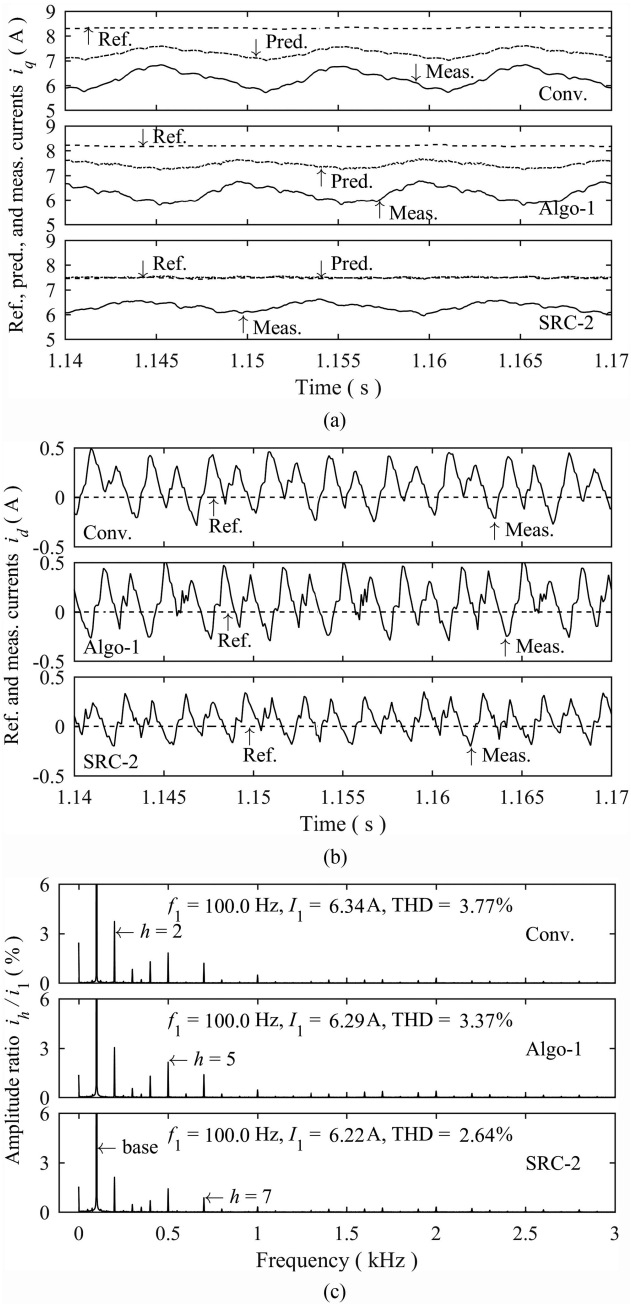

Fig. 11. Experimental stator current and frequency spectrum with injected current distortion ($n = 1500$ r/min). (a) Current i_q in q-axis. (b) Current i_d in d-axis. (c) Frequency spectrum.

compensating, thus, the proposed SRC-2 method enhances the system's robustness against current disturbances. Besides, similar to the simulation results as presented in Section IV, Algo-1 eliminates parts of the harmonics with limited improvements, whereas SRC-2 significantly decreases all harmonics listed in Table IV and it outperforms Algo-1 and the conventional MPC with the least harmonics. The THD of stator current is reduced from 3.77% (Conv.) and 3.37% (Algo-1) to 2.64% for the proposed SRC-2, i.e., SRC-2 produces performance enhancement with 30.0% and 21.7% reduction of THD compared with the conventional MPC and Algo-1, respectively.

TABLE IV
EXPERIMENTAL CURRENT FREQUENCY SPECTRUMS (%) OF STATOR CURRENT WITH INJECTED CURRENT DISTORTION ($I_L = 6.3$ A, $N = 1500$ r/min)

Controller	DC	2nd	4th	5th	7th
Conv.	2.45	3.74	1.32	1.83	1.20
Algo-1	1.37	3.04	1.29	2.15	1.37
SRC-2	1.34	2.00	0.69	1.40	0.87
Controller	11th	13th	17th	19th	THD
Conv.	0.08	0.10	0.20	0.15	3.77
Algo-1	0.06	0.26	0.36	0.29	3.37
SRC-2	0.05	0.10	0.24	0.16	2.64

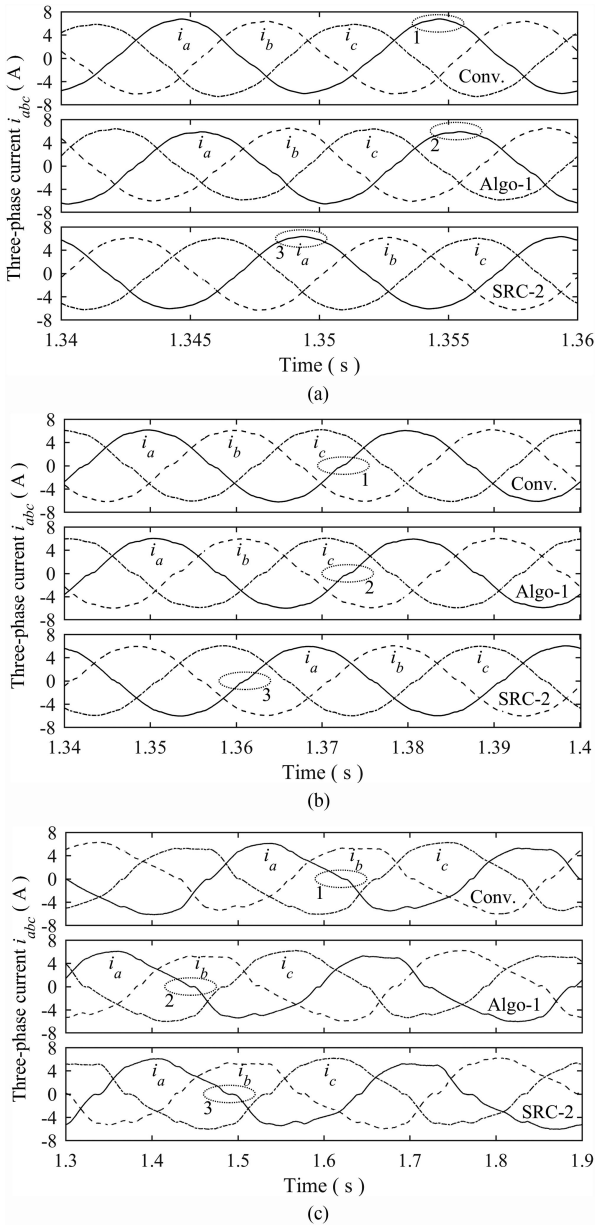

Fig. 12. Experimental three-phase stator current with injected current distortion. (a) $n = 1500$ r/min. (b) $n = 500$ r/min. (c) $n = 50$ r/min.

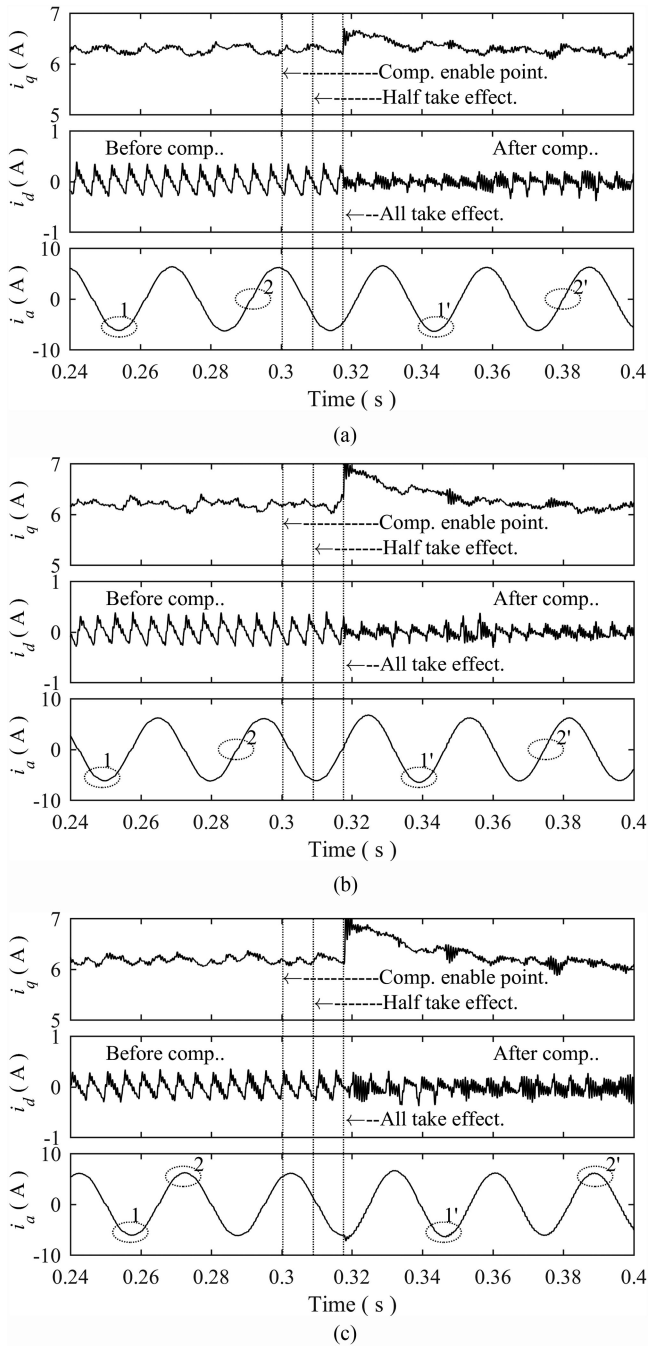

Fig. 13. Experimental stator current before and after compensating using SRC-2 with parameter mismatch ($n = 500$ r/min). (a) Case 1: $4.0R_s$. (b) Case 2: $0.85L_s$. (c) Case 3: $0.85\Phi_m$.

The experimental three-phase stator currents for the three MPCs with injected current distortion are presented in Fig. 12(a) with speed command $n = 1500$ r/min, in Fig. 12(b) with $n = 500$ r/min, and in Fig. 12(c) with $n = 50$/r/m, respectively. All methods are compared under the same load 6.3 A, and for high-speed regions such as 1500 and 500 r/min, SRC-2 produces the least current distortion compared with Algo-1 and the conventional MPC as the markers "1," "2," and "3" show. For lower speeds such as 50 r/min as shown in Fig. 12(c), the proposed SRC-2 method is essentially the same as the Algo-1 method.

TABLE V
EXPERIMENTAL THD (%) OF STATOR CURRENT FOR SRC-2 WITH PARAMETER MISMATCH ($N = 500$ r/min)

Para. mismatch	Before comp.		After comp.	
	Base (A)	THD (%)	Base (A)	THD (%)
Case 1: $4.0R_s$	6.28	2.72	6.26	1.48
Case 2: $0.85L_s$	6.20	2.81	6.12	1.75
Case 3: $0.85\Phi_m$	6.17	2.62	6.14	1.86

Moreover, the proposed SRC-2 with mismatched parameters including the stator resistance R_s, stator inductance L_s, and magnet flux ϕ_m as shown in (41) are separately verified through experiment, and the results are presented in Fig. 13(a)–(c), respectively. The THD of stator current of SRC-2 before and after compensating are presented in Table V. Similar to the simulation process, the compensation provided by SRC-2 is suddenly added to the system at 0.3 s. According to the experimental results, the current ripple and distortion introduced by parameter mismatches are well compensated as Fig. 13 and Table V show.

VI. CONCLUSION

The performance of the conventional MPC-based PMSM drive system will be deteriorated due to the existence of external disturbances. The effects caused by certain kinds of disturbances such as parameter mismatch, current distortion, and deadtime effects are theoretically analyzed. And then, the SRC method based on the internal model theory is proposed to improve the system robustness. In which, an open-loop SRC-2 controller with the first and second resonant unit is utilized, and moreover, the output filter is designed to ensure system stability and to correct the quantizing error of frequency. Finally, a robust MPC for PMSM drive system with the proposed SRC-2 method is implemented, and the feasibility and effectiveness are validated through both simulation and experiment. When the PMSM starts from standstill, the proposed SRC-2 method responds fast and it just needs 60% of time used by the conventional MPC to reach the reference speed. And in the steady-state, it shows 30% and 22% reduction in THD of stator current compared with the conventional MPC and Algo-1 method, respectively.

REFERENCES

[1] S. Almer, S. Mariethoz, and M. Morari, "Dynamic phasor model predictive control of switched mode power converters," *IEEE Trans. Control Syst. Technol.*, vol. 23, no. 1, pp. 349–356, Jan. 2015.
[2] J. Scoltock, T. Geyer, and U. K. Madawala, "A comparison of model predictive control schemes for MV induction motor drives," *IEEE Trans. Ind. Informat.*, vol. 9, no. 2, pp. 909–919, May 2013.
[3] C. Wang, C. J. Ong, and M. Sim, "Model predictive control using segregated disturbance feedback," *IEEE Trans. Autom. Control*, vol. 55, no. 4, pp. 831–840, Apr. 2010.
[4] L. Tarisciotti, P. Zanchetta, A. Watson, P. Wheeler, J. C. Clare, and S. Bifaretti, "Multi-objective modulated model predictive control for a multilevel solid-state transformer," *IEEE Trans. Ind. Appl.*, vol. 51, no. 5, pp. 4051–4060, Sep./Oct. 2015.

[5] L. Tarisciotti, P. Zanchetta, A. Watson, J. C. Clare, M. Degano, and S. Bifaretti, "Modulated model predictive control for a three-phase active rectifier," *IEEE Trans. Ind. Appl.*, vol. 51, no. 2, pp. 1610–1620, Mar./Apr. 2015.
[6] M. H. Vafaie, B. M. Dehkordi, P. Moallem, and A. Kiyoumarsi, "A new predictive direct torque control method for improving both steady-state and transient-state operations of the PMSM," *IEEE Trans. Power Electron.*, vol. 31, no. 5, pp. 3738–3753, May 2016.
[7] F. Niu, K. Li, and Y. Wang, "Direct torque control for permanent-magnet synchronous machines based on duty ratio modulation," *IEEE Trans. Ind. Electron.*, vol. 62, no. 10, pp. 6160–6170, Oct. 2015.
[8] T. Geyer and D. E. Quevedo, "Performance of multistep finite control set model predictive control for power electronics," *IEEE Trans. Power Electron.*, vol. 30, no. 3, pp. 1633–1644, Mar. 2015.
[9] Z. Mynar, L. Vesely, and P. Vaclavek, "PMSM model predictive control with field-weakening implementation," *IEEE Trans. Ind. Electron.*, vol. 63, no. 8, pp. 5156–5166, Aug. 2016.
[10] J. I. Leon and L. G. Franquelo, "Predictive optimal switching sequence direct power control for grid-connected power converters," *IEEE Trans. Ind. Electron.*, vol. 62, no. 4, pp. 2010–2020, Apr. 2015.
[11] M. Siami, D. A. Khaburi, A. Abbaszadeh, and J. Rodríguez, "Robustness improvement of predictive current control using prediction error correction for permanent-magnet synchronous machines," *IEEE Trans. Ind. Electron.*, vol. 63, no. 6, pp. 3458–3466, Jun. 2016.
[12] K. H. Kim and M. J. Youn, "A simple and robust digital current control technique of a PM synchronous motor using time delay control approach," *IEEE Trans. Power Electron.*, vol. 16, no. 1, pp. 72–82, Jan. 2001.
[13] K. X. Yang *et al.*, "An adaptive deadtime compensation method based on predictive current control," presented at *the IEEE 8th Int. Conf. Power Electron. Motion Control*, Hefei, China, May 22–26, 2016.
[14] T. Turker, U. Buyukkeles, and A. F. Bakan, "A robust predictive current controller for PMSM drives," *IEEE Trans. Ind. Electron.*, vol. 63, no. 6, pp. 3906–3914, Jun. 2016.
[15] J. L. Lee and T. H. Liu, "Implementation of a predictive controller for a sensorless interior permanent-magnet synchronous motor drive system," *IET Elect. Power Appl.*, vol. 6, no. 8, pp. 513–525, Sep. 2012.
[16] M. Preindl, "Robust control invariant sets and Lyapunov-based MPC for IPM synchronous motor drives," *IEEE Trans. Ind. Electron.*, vol. 63, no. 6, pp. 3925–3933, Jun. 2016.
[17] M. S. Rafaq, F. Mwasilu, J. Kim, H. H. Choi, and J.-W. Jung, "Online parameter identification for model-based sensorless control of interior permanent magnet synchronous machine," *IEEE Trans. Power Electron.*, vol. 32, no. 6, pp. 4631–4643, Jun. 2017.
[18] D. Chen, J. M. Zhang, and Z. M. Qian, "Research on fast transient and $6n \pm 1$ harmonics suppressing repetitive control scheme for three-phase grid-connected inverters," *IET Power Electron*., vol. 6, no. 3, pp. 601–610, Mar. 2013.
[19] A. H. M. Sayem, Z. W. Cao, and Z. H. Man, "Model free ESO-based repetitive control for rejecting periodic and aperiodic disturbances," *IEEE Trans. Ind. Electron.*, vol. 64, no. 4, pp. 3433–3441, Apr. 2017.
[20] A. Trivedi and M. Singh, "Repetitive controller for VSIs in droop-based AC-microgrid," *IEEE Trans. Power Electron.*, vol. 32, no. 8, pp. 6595–6604, Aug. 2017.
[21] K. H. Cho, J. H. Kim, S. B. Choi, and S. Oh, "A high-precision motion control based on a periodic adaptive disturbance observer in a PMLSM," *IEEE Trans. Mechatronics*, vol. 20, no. 5, pp. 2158–2171, Oct. 2015.
[22] R. Cao and K. S. Low, "A repetitive model predictive control approach for precision tracking of a linear motion system," *IEEE Trans. Ind. Electron.*, vol. 56, no. 6, pp. 1955–1962, Jun. 2009.
[23] Q. S. Zhao *et al.*, "Improved repetitive control scheme for grid-connected inverter with frequency adaptation," *IET Power Electron*., vol. 9, no. 5, pp. 883–890, Apr. 2016.
[24] Q. Z. Yan, X. J. Wu, X. B. Yuan, and Y. Geng, "An improved grid-voltage feedforward strategy for high-power three-phase grid-connected inverters based on the simplified repetitive predictor," *IEEE Trans. Power Electron.*, vol. 31, no. 5, pp. 3880–3897, May 2016.
[25] Y. H. Yang, K. L. Zhou, and F. Blaabjerg, "Enhancing the frequency adaptability of periodic current controllers with a fixed sampling rate for grid-connected power converters," *IEEE Trans. Power Electron.*, vol. 31, no. 10, pp. 7273–7285, Oct. 2016.
[26] M. A. Herran, J. R. Fischer, S. A. Gonzalez, M. G. Judewicz, I. Carugati, and D. O. Carrica, "Repetitive control with adaptive sampling frequency for wind power generation systems," *IEEE J. Emerg. Sel. Topics Power Electron*., vol. 2, no. 1, pp. 58–69, Mar. 2014.
[27] P. L. Cui, Q. R. Wang, S. Li, and Q. Gao, "Combined FIR and fractional-order repetitive control for harmonic current suppression of magnetically suspended rotor system," *IEEE Trans. Ind. Electron.*, vol. 64, no. 6, pp. 4828–4835, Jun. 2017.
[28] Z. X. Zou *et al.*, "Fractional-order repetitive control of programmable AC power sources," *IET Power Electron*., vol. 7, no. 2, pp. 431–438, Feb. 2014.
[29] C. Xie, X. Zhao, M. Savaghebi, L. Meng, J. M. Guerrero, and J. C. Vasquez, "Multirate fractional-order repetitive control of shunt active power filter suitable for microgrid applications," *IEEE J. Emerg. Sel. Topics Power Electron*., vol. 5, no. 2, pp. 809–819, Jun. 2017.

Ying Liu was born in Hubei Province, China, in 1988. He received the B.S. degree from the School of Automation, Huazhong University of Science and Technology, Wuhan, China, in 2012. He is currently working toward the Ph.D. degree at the School of Automation, Huazhong University of Science and Technology.

His research interests include power convertors and high-performance ac-motor control strategies.

Shanmei Cheng was born in Hubei Province, China, in 1966. He received the B.S. degree from the School of Naval Architecture and Ocean Engineering, and the M.S. and the Ph.D. degrees from the School of Automation, Huazhong University of Science and Technology, Wuhan, China, in 1988, 1991, and 2002, respectively.

From 2002 to 2005, he was a Postdoctoral Fellow with the School of Mechanical Science and Engineering, Huazhong University of Science and Technology. From 2006 to 2007, he was a Visiting Professor with the Department of Electrical and Computer Engineering, University of Toronto, Toronto, Canada. Since 2003, he has been a Full Professor with the School of Automation, Huazhong University of Science and Technology. He has authored or coauthored more than 100 technique papers and authored two books. His research interests include adjustable speed drives, power electronics, control theory, and DSP and microcontroller application.

Bowen Ning was born in Hubei Province, China, in 1987. He received the B.S. degree from the Wuhan University of Science and Technology, Wuhan, China, in 2009, and the Ph.D. degree from the Huazhong University of Science and Technology, Wuhan, in 2016.

He is currently a Lecturer with the School of Information Science and Engineering, Wuhan University of Science and Technology. His research interests include high-performance ac-motor drivers and power convertors.

Yesong Li was born in Hunan Province, China, in 1970. He received the B.S. and Ph.D. degrees from the School of Automation, Huazhong University of Science and Technology, Wuhan, China, in 1990 and 1996, respectively.

From 1998 to 2000, he was a Research Associate with the Department of Electrical and Electronic Engineering, Hong Kong University of Science and Technology, Hong Kong. Since 2004, he has been a Full Professor with the School of Automation, Huazhong University of Science and Technology. His research interests include high-performance ac-motor drivers and field bus network control technology for industrial application.